Exploring the modulation of extracellular metabolites in different *Listeria monocytogenes* strains under cold-stress

Hyun-Jun Kim[1¶], Hye-Jin Kim[1¶], Cheorun Jo[1, 2*]

[1] Department of Agricultural Biotechnology, Center for Food and Bioconvergence, and Research Institute of Agriculture and Life Science, Seoul National University, Seoul 08826, Republic of Korea

[2] Institute of Green BioScience and Technology, Seoul National University, Pyeongchang 25354, Republic of Korea

[¶]These authors contributed equally to this work.

Running title: Extracellular metabolites of Listeria monocytogenes under cold-stress

* Corresponding author

Name: Cheorun Jo

Affiliation: Department of Agricultural Biotechnology, Center for Food and Bioconvergence, and Research Institute of Agriculture and Life Science, Seoul National University, Seoul 08826, Republic of Korea

City: Seoul

Zip code: 08826

Country: Republic of Korea

Telephone: +82-2-880-4804

Fax: +80-2-873-2271

E-mail: cheorun@snu.ac.kr

Exploring the modulation of extracellular metabolites in different *Listeria monocytogenes* strains under cold-stress

Abstract

This study investigated the modulation of extracellular metabolites in *Listeria monocytogenes* NCCP 15743 (L5), NCCP 16594 (L6), and ATCC 19111 (L9) strains in cold-stressed culture. The strains were cultured in Mueller Hinton broth at 8℃ for 22 days. Extracellular metabolites were extracted at five growth phases (initial, lag, log, early saturate, and saturate) of each strain. Under cold-stress, growth phases of L5 and L6 exhibited similarities, while L9 displayed a distinct pattern. The change in extracellular metabolites under cold-stress was dependent on growth phase and strain. The presence of *L. monocytogenes* was distinguished based on the concentrations of trehalose, isoleucine, arginine, and phenylalanine. During extended cold-stressed culture, all strains enhanced two metabolic pathways at the lag and log phases: energy metabolism (trehalose, lactate, propanoate, acetate, ethanol, and formic acid) and glutathione-related metabolism (acetate, histidine, arginine, proline, glutamate, glycine, serine, and methionine). The expression of these extracellular metabolites provides crucial insights into the complex metabolic adaptations of *L. monocytogenes* during cold-stress culture. This study introduces a distinctive approach to identifying *L. monocytogenes* under cold-stress, offering potential application for safety enhancement in the food industry.

Keywords: Extracellular metabolites, Multivariate analysis, Culture media, Foodborne pathogens detection method, Nuclear magnetic resonance spectroscopy

Introduction

Food poisoning can be caused by consuming food that is contaminated with pathogenic bacteria, parasites, viruses, or toxins (Dewey-Mattia, 2018). According to the CDC (Centers for Disease Control and Prevention) (Dewey-Mattia, 2018), approximately 9 million people in the United States experience food poisoning each year due to contaminated foods. Of those, 3.6 million cases are attributed to bacteria, leading to 36,000 hospitalizations and 1,093 deaths annually (Dewey-Mattia, 2018). Major food poisoning outbreaks have been attributed to animal-origin foods (AOF), affecting approximately 4 million people annually (Painter et al., 2013). Therefore, research on methods for continuous monitoring of pathogenic bacteria in AOF is essential for ensuring food safety.

To ensure the microbial safety of AOF, a cold chain system is employed (Bassey et al., 2021). This system involves the transportation of food while sustaining a low-temperature environment, usually ranging between 2 and 8 ℃. Maintaining a low temperature induces cold stress on microorganisms, leading to delayed growth and eventual death (Yu et al., 2023). Cold-stress reduces lipid bilayer fluidity, impairing membrane structural integrity and other cell membrane-related functions of bacteria (Bassey et al., 2021). Additionally, it leads to the increase of instability of RNA and DNA secondary structures, as well as the destabilization of cellular macromolecules, particularly ribosomes (Bassey et al., 2021). However, *Listeria monocytogenes* (LM), a gram-positive, rod-shaped, non-spore-forming bacterium, can adapt to a wide range of temperatures (0-45 ℃) (Yoon et al., 2022). Based on its high environmental adaptability, LM is commonly detected in foods such as meat and fish, unpasteurized milk, and ready-to-eat foods. It has the potential for contamination across various steps of food processing, distribution, and storage environments (Kramarenko et al., 2013). Consequently, LM has been reported to cause the highest hospitalization rate (91%) compared to other known foodborne pathogens in the United States upon infection (Dewey-Mattia, 2018). Thus, from the food safety standpoint, it is very important to understand metabolism of LM during cold-stress in managing its presence in refrigerated food such as AOFs.

Metabolomics could be used to investigate small molecules (<1.5 kDa) released from microbes for understanding their metabolic processes, both intracellular and extracellular (Aung et al., 2023). Intracellular metabolomics involves the study of metabolites within microbial cells that undergo changes during growth and differentiation. This encompasses metabolites located within mechanical barriers, cell membranes, or cell envelopes (Pinu et al.,

2017). On the other hand, extracellular metabolomics explores metabolites that microbial cells secrete into the environment or culture medium (Pinu and Villas-Boas, 2017). Since extracellular metabolites are by-products of the intracellular metabolic activities of microorganisms, they can serve as indicators of microbial growth in specific environments, encompassing outcomes both intracellular and extracellular metabolism (Pinu and Villas-Boas, 2017). The metabolism of central carbon, energy production, amino acid supply, and protein synthesis varies depending on the microbial species and environment in which they grow (Chubukov et al., 2014; Kim et al., 2021). Especially, in foods like AOFs, changes in bacterial intracellular metabolism can result in modifications of various extracellular metabolites, affecting AOFs quality through alterations in parameters such as pH and amino acid composition (Kim et al., 2022a). Therefore, given the significant correlation between intracellular and extracellular metabolites (Pinu et al., 2017), measuring extracellular metabolites allows for a comprehensive understanding of both the microorganisms and the conditions of AOFs. In our previous study, we identified the presence, species, and quantity of pathogenic microorganisms by analyzing extracellular metabolites present in the media (Kim et al., 2022b). Moreover, the method of analyzing extracellular metabolites is easy compared with intracellular metabolites (Pinu and Villas-Boas, 2017). This approach, when applied to studying LM, could help to enhance the safety of AOFs by providing critical basic information at the point of the metabolic change of pathogens.

Therefore, we aimed to investigate the extracellular metabolite profiles in 3 strains of LM under cold-stress. Furthermore, we evaluated the change in metabolic patterns of LM during exposure to cold-stress. Finally, we attempted to introduce a new approach for identifying LM responses to cold-stress through the analysis of extracellular metabolites.

Materials and Methods

Materials

Tryptic Soy broth, Tryptic Soy agar, Mueller Hinton broth, and 3-(trimethylsilyl) propionic-2,2,3,3-d4 acid (TSP) were purchased from Sigma-Aldrich (Mannheim, Germany). Perchloric acid and potassium hydroxide were purchased from Duksan Pure Chemical Co. (Ansan, Korea). Deuterium oxide (D_2O) was purchased from Eurisotop (Saint-Aubin Cedex, France).

Bacterial strains, growth conditions, and preparation of the inoculum

The investigated *L. monocytogenes* (LM) strains (NCCP 15743, NCCP 16594 and ATCC 19111) were obtained as clinical isolates from the National Culture Collection for Pathogens (NCCP, Korea) and American Type Culture Collection (ATCC). Details of the clinical isolates of LM are provided in Table S1. Each strain was preserved at -80℃ in 40%(vol/vol) glycerol. For resuscitation, strains were cultured in 25 mL of tryptic soy broth and incubated at 37℃ for 24 hrs. The cultures were then streaked onto tryptic soy agar places and incubated at 37℃ for 24 hrs. The single colonies were transferred to Mueller Hinton broth and incubated at 37℃ for 18 hrs. After incubation, the cultures were centrifuged at 3,000 ×g for 10 min. The pelleted cells were washed twice with saline solution and adjusted to an optical density of 0.1 at 600 nm to standardize the bacterial concentration. These cells were further diluted to a final concentration using a dilution factor of 1×10^7 with saline solution. Finally, 0.1 mL of each diluted bacterial strain was introduced into 9.9 mL of Mueller Hinton broth to achieve an initial count of approximately 1 log CFU/mL. Mueller Hinton broth without any inoculation served as the control (labeled M), while broths inoculated with LM strains NCCP 15743, NCCP 16594, and ATCC 19111 were labeled L5, L6, and L9, respectively. All samples were immediately placed in an 8℃ incubator after preparation and incubated for up to 22 days. The temperature of 8℃ was selected because it is a typical temperature used in domestic refrigerators (Roccato et al., 2015) and has been used in previous studies on meat storage under cold conditions (Kaur et al., 2021; Mataragas et al., 2006; Park et al., 2008; Sørheim et al., 1999).

Population of microorganism and sampling

Microbial growth for each strain was measured at 24 hrs intervals, starting after the initial 5 days, with measurements replicated 3 times at each time point (n = 3). The characterization of microbial growth phases (initial, lag, log early saturate, and saturate phase) was based on the growth curves (Willey et al., 2013). A microbial population reaching approximately 3 log CFU/mL was identified as being in the lag phase, indicating adaptation to the culture medium. When the population reached approximately 7 log CFU/mL during exponential growth, it was considered to be in the log phase. Completion of exponential growth marked the transition to the early saturation phase, and samples that remained in saturation for an additional 2 days were categorized as being in the saturation phase. Metabolites were extracted from all strains when they reached each designated growth phase (early, late, log supersaturated, and saturated

phases), with extractions performed from 5 separate culture tubes prepared for each phase (n = 5). Selected samples for metabolite extraction underwent centrifuged at 12,000 ×g for 20 min. The supernatant was then filtered through a 0.22 µm syringe filter (PTFE, Corning, NY, USA) and plated on a non-selective medium to ensure the absence of cells. The cell-free supernatant was then stored at -80 ℃ until metabolite extraction.

Polar metabolites extraction procedure

The procedure for extracting polar metabolites was based on the method described by Kim et al. (2021). Initially, 5 mL of filtered media was combined with 5 mL of pre-cooled 0.6 M perchloric acid and vortex-mixed for 1 min. The mixture was then centrifuged (Continent 512R, Hanil Co., Ltd., Incheon, Korea) at 3,000 ×g for 20 min. The supernatant was transferred to a new test tube and neutralized to a pH of 7.0 using 1 M potassium hydroxide. After neutralization, the sample was centrifuged again under the same conditions, filtered (Whatman No. 1, Whatman PLC., Buckinghamshire, UK), and subsequently lyophilized (Freeze Dryer 18, Labco Corp., Kansas City, MO, USA) in preparation for nuclear magnetic resonance (NMR) analysis.

Metabolites measurement using Nuclear Magnetic Resonance spectroscopy

Polar metabolites were identified and quantified using an 850 MHz cryo-NMR spectrometer (Bruker Biospin GmbH, Rheinstetten, Germany). The lyophilized extracts were reconstituted in 1 mL of D_2O (20 mM phosphate buffer, pH 7.0) with an internal standard [1 mM 3-(trimethylsilyl) propionic-2,2,3,3-d4 acid (TSP)]. The reconstituted samples were then warmed in a water bath at 35℃ for 10 min. Following centrifugation at 17,000 ×g for 10 min, the supernatant was transferred into a 5 mm NMR tube for NMR analysis.

NMR spectra were acquired in D_2O at 298 K using an 850 MHz cryo-NMR spectrometer. A modified standard zg30 pulse sequence (with a recycle delay of 1 sec) was employed for one-dimensional 1H NMR analysis in Topspin 4.1.1 (Bruker). This sequence was executed with 64K data points, a sweep width of 17,007.803 Hz, and 128 scans. The chemical shifts (δ) were calibrated relative to the TSP resonance, and manual adjustments were made for baseline corrections. As described by Kim et al. (2021), metabolite identification utilized heteronuclear single quantum coherence (HSQC), correlation spectroscopy (COZY) and Chenomx deconvolution programs. The HSQC was conducted with 2 K data points in the t_2 domain and

512 increments in t_1, each with 8 and 32 scans, respectively. COZY were performed with 2 K data points in t_2 domain and 256 increments in t_1 with 8 scans. The spectral widths were set at 12.0016 ppm for the f_2 dimension and 180.0045 ppm for the f_1 dimension. A coupling constant value of 145 Hz was used to define the delay duration for the short-range correlations. Using 1 mM TSP as the internal standard, metabolite quantification was achieved. The following equation was used for quantifying the concentrations of metabolites:

$$\text{Concentration (g/mL)} = \left[\frac{Numbers\ of\ proton\ (internal\ standard)}{Numbers\ of\ proton\ (metabolite)} \times \frac{Intesitiy\ of\ peak\ (metabolite)}{Intensity\ of\ peak\ (internal\ standard)} \times Concentration\ (interanl\ standard)\right] \div Sample\ volume$$

Data processing and statistical analysis

Partial least squares-discriminant analysis (PLS-DA) was utilized as a multivariate analysis technique to optimize the separation between different groups (Allen et al., 2019). PLS-DA recognizes class labels and combines individual variates to reduce dimensionality (Allen et al., 2019). For extracellular metabolite results, the changing pattern of LM during the incubation period and metabolic differences between strains (L5, L6, L9) were confirmed using the PLS-DA model. Prior to conducting the multivariate and pathway analyses, the quantified data were subjected to a log10 transformation and autoscaling to normalize the distribution and scale of the variables. The differentiation in metabolic patterns observed over the incubation period and between the strains was further analyzed using orthogonal partial least squares-discriminant analysis (OPLS-DA) (Galindo-Prieto et al., 2014).

Pathway analysis was performed according to Xia and Wishart (2011), focusing on the comparison between the baseline (day 0) and each growth phase (lag, log, early saturate, saturate), respectively. The Human Metabolome Database (HMDB) (www.hmdb.ca) ID of each metabolite was used, and the annotated metabolome pathway was cross-referenced with the Kyoto Encyclopedia of Genes and Genomes (KEGG) pathway database. Multivariate analysis (PLS-DA and OPLS-DA) and pathway analysis was performed on MetaboAnalyst 5.0 (www.metaboanalyst.ca). Significant differences in the identified metabolites were determined

using the Tukey's multiple range test, executed with SAS software (SAS 9.4, SAS Institute, Cary, NC, USA), with a confidence level set at $P < 0.05$.

Results and Discussion

Cold-stress culture growth curves of LM

The three LM strains were cultured under the cold-stress conditions. All strains were initially inoculated at an average concentration of 1 log CFU/mL. Throughout the duration of the cold-stressed culture, all strains proliferated and reached a concentration of 8 log CFU/mL (Fig 1). To assess the growth patterns of each LM strain across different phases, we identified five distinct phases (initial, lag, log, early saturation, and saturation) based on the LM growth curve (Willey et al., 2013). Initial phase refers to the inoculation period where the bacterial concentration is at or around 1 log CFU/mL. Lag phase is the period following inoculation during which bacteria adapt to growth conditions but have not yet begun to proliferate, characterized by a slow or negligible increase in cell numbers (Willey et al., 2013). To investigate changes in extracellular metabolites during the lag phase, we cultured the bacteria until they reached a concentration of 3 log CFU/mL. The growth patterns of L5 and L6 differed from that of L9. L5 and L6 reached the lag phase on day 4, however, L9 reached it on day 6. The log phase is characterized by exponential growth, with bacteria rapidly multiplying and the population size increasing significantly (Willey et al., 2013). Accordingly, we selected the 7 log CFU/mL to profile the extracellular metabolites during log phase. L5 and L6 showed similar exponential growth, reaching about 7 log CFU/mL on day 9. However, L9 was approximately 7 log CFU/mL on day 18. As the resources become limited, the growth rate starts to decelerate (Willey et al., 2013), signaling the early saturate phase. L5 and L6 reached the saturation on day 12, while L9 reached it on day 20. To assess the impact of reaching saturation, we continued to cultivate the cultures for 2 days beyond the point of early saturation. In the log phase, doubling times of L5, L6, and L9 were 11.25, 10.15, and 20.37 hrs, respectively. Cordero et al. (Cordero et al., 2016) reported that the doubling time of LM at 8℃ varied between strains (5-14 hrs). This finding is in line with previous results, where the doubling times of different strains (Scott A, CA, V37CE, and V7) of LM in skim milk were 12.5, 13.25, 14.25, and 10 hrs, respectively, when cultured at 8℃ (Rosenow et al., 1987). The result demonstrates that each strain exhibits different growth patterns in media under cold-

stress. Consequently, the extracellular metabolites were measured to confirm metabolic patterns according to the growth phase and population at day 0, 4, 6, 9, 12, 14, 18, 20, and 22.

Qualitative analysis of metabolites in culture media

A total of 32 metabolites were identified and quantified (S2 Table). Although the metabolite profiles of the three strains showed similarities across all phases, the concentration of certain metabolites varied. The quantitative results of the analysed metabolites for each strain are presented in Tables S3, S4, and S5. PLS-DA was employed to examine the trends based on these quantitative results (Fig 2). Each strain exhibited distinct patterns over the culture period. In strains L5 and L6, the extracellular metabolite profile shifted along four vectors (day 0-4, day 4-9, day 9-18, and day 18-22; Fig 2a-b), whereas this pattern was different in L9 (day 0-4, day 4-18, and day 18-22; Fig 2c). These segments correlate with the growth phases observed in the growth curve (Fig 1), suggesting that the alterations in metabolomic patterns were attributed to unique metabolic activities occurring within each growth phase (Robador et al., 2018). Similarly, Hain et al. (2008) reported that the stress response metabolism of LM was differentially regulated according to the bacterial growth phase.

Common or unique metabolic patterns of LM strains (L5, L6, and L9) in the cold-stressed culture have been identified (Fig 3). OPLS-DA was conducted between samples at the end of each vector and metabolites distinguishing each vector were expressed by their VIP scores (VIP > 1.0). Metabolites such as arginine, carnosine, ethanol, phenylalanine, threonine, and tyrosine were identified in VIP score chart, discriminating the day 0 vs 4 vector across all three strains (Fig 3a, 3e, 3i), corresponding to the lag phase (Fig 1). The day 4 vs 9 vector in L5 and L6 corresponded to period range from lag phase to log phase (Fig 1). The day 9 vs 18 vector represented the range from log phase to saturation phase in L5 and L6 (Fig 1). Meanwhile, L9 had the range of lag phase to log phase corresponded to the day 4 vs 18 vector (Fig 3). Formate, leucine, serine, threonine, trehalose, and tyrosine were plotted in VIP score chart among the day 4 vs 9, day 9 vs 18, and day 4 vs 18 vectors (Fig 3b, 3c, 3f, 3g, 3j). The day 18 vs 22 vector was distinguished by methanol and proline for all three strains, which corresponded to the log phase (for L5, L6) and saturation phase (for L5, L6, L9). Thus, the change in metabolites in LM under cold-stress was characterized by different growth stages and strains.

Comparison of extracellular metabolites of LM strains in the cold-stressed culture

Metabolite profiling serves as a valuable tool for distinguishing between strains, similar to techniques like multiplex PCR, which is commonly used to distinguish LM serotypes (Doumith et al., 2004). In this study, PLS-DA was conducted to investigate the influence of different LM strains (L5, L6, L9) on extracellular metabolites under cold-stress, using samples from each strain at the saturated point (an additional two days following the attainment of a concentration of 8 log CFU/mL). As shown in Fig 4, component 1 effectively distinguished the un-inoculated sample (M) from all three strains. In contrast, differences among the strains were predominantly driven by components 2 and 3. Since trehalose, isoleucine, arginine, and phenylalanine were only found in VIP score plot of component 1, these extracellular metabolites may contribute to detecting the presence of every LM strain in this study. Meanwhile, the contents of lactate, glycerol, acetate, methanol, asparagine, proline, ethanol, and glutamate, which were used in component 2 and 3 (VIP>1), contributed to the differences among strains. Trehalose, a disaccharide composed of two glucose molecules, serves as an energy source through glycolysis and can resist oxidative stress by interacting with fatty acids featuring cis double bonds (Vanaporn and Titball, 2020). The essential amino acids (isoleucine, arginine, and phenylalanine) are employed as nutrients primarily for cell growth and metabolism (Sauer et al., 2019). Previous reports have suggested that isoleucine, arginine, and phenylalanine enhance the growth of LM (Sauer et al., 2019). Differences among LM strains may be due to their genomic diversity, which can lead to variations in metabolite production (Nightingale et al., 2005). As a result, trehalose, isoleucine, arginine, and phenylalanine significantly influenced the distinction between un-inoculated culture medium and LM inoculated (L5, L6, and L9) clusters, regardless of the strain. Meanwhile, lactate, glycerol, acetate, methanol, asparagine, proline, ethanol, and glutamate exhibited differential utilization based on the specific strains.

Pathway analysis using the extracellular metabolites of LM

Metabolic pathway analysis was conducted using the 32 metabolites identified in L5, L6, and L9 strains, as shown in Fig 5. This analysis verified the significant involvement of energy and glutathione metabolic pathways of LM in the cold-stressed culture. The marked metabolites identified in this study aligned with energy metabolic pathways, including carbohydrate metabolism (glycolysis/gluconeogenesis and glyoxylate, dicarboxylate metabolism, and pyruvate metabolism), propanoate metabolism, and methane metabolism (Fig

5a). Specifically, carbohydrate metabolism and propanoate metabolism showed enhanced expression during the lag and log phases in all strains. Meanwhile, the expression of methane metabolism was enhanced during the early saturate and saturate phase. The increase in carbohydrate metabolism during the lag and log phases might be attributed to the adaptation to environmental stressors (Aertsen and Michiels, 2004). This adaptation might be due to metabolic reactions involving propionyl CoA, and changes in the fatty acid composition of the cell membrane (Rinehart et al., 2018). These changes might help the organism adjust to different nutrient levels and stress conditions (Rinehart et al., 2018). Most of glutathione-related metabolism, including pathways such as glutathione metabolism, D-glutamine and D-glutamate metabolism, arginine and proline metabolism, arginine biosynthesis, glyoxylate and discarboxylate metabolism, alanine, aspartate and glutamate metabolism, histidine metabolism, cysteine and methionine metabolism, and glycine, serine and threonine metabolism, showed enhanced expression during the lag and log phases in all strains (Fig 5a). Meanwhile, sulfur metabolism was expressed more highly in the early saturate and saturate phases, indicating potential upregulation during later growth phases. Under cold stress, glutathione might show strong expression as it is used to degrade superoxide by glutathione peroxidase (Sibanda and Buys, 2022). The degree of expression was different for each strain (Fig 5a). The energy and glutathione related metabolism exhibited strong expression at the lag phase of L6 and L9, while L5 at the log phase. This is because the stress response metabolism of LM is regulated differently depending on the bacterial strain (Hain et al., 2008). In L9, the overall metabolic expression level was lower than those of L5 or L6 (Fig 5a), because its growth rate was slower (Fig 1). Therefore, it was confirmed that energy metabolism and glutathione metabolism were primarily activated in LM during cold-stress.

An overview of critical metabolic pathways and extracellular metabolites was created to examine the response of LM to cold-stressed culture (Fig 5b and 5c). In the energy-related pathway, significant changes in trehalose, lactate, formate, acetate, and propanoate were confirmed during cold-stress (Fig 5b, S3-5 Table). In all strains trehalose levels decreased, while formate and acetate increased as the cold-stressed culture period progressed. Lactate concentration was high in the log phase in L5 and L6, but no significant increase in L9 was observed in different phases during the cold-stressed culture (S3-5 Table). Propanoate was significantly higher in the log phase of L5, and in the lag phase of L6, while its concentration in L9 significantly decreased over the culture period (S3-5 Table). Trehalose, composed of two glucose units, is broken down into glucose molecules through glycolysis to be used for energy

(Rinehart et al., 2018; Schär et al., 2010). From the breakdown of glucose, LM produces lactate anaerobically and acetate aerobically, deriving energy in the process (Garvie, 1980). Glucose obtained from trehalose breakdown could produce energy through pyruvate metabolism (Rinehart et al., 2018; Schär et al., 2010). 2-Oxobutanoate can be catabolized to propionyl CoA by propionate metabolism, and propionyl CoA is catabolized to propionate to generate ATP (Gonzalez-Garcia et al., 2017).

In this study, a rise in the concentration of distinct metabolites associated with glutathione metabolism was noted during the log phase in L5 and the lag phase in L6 (Fig 5c). These metabolites encompassed metabolites related to glutamate production (histidine, arginine, and glycine), metabolites related to L-cysteine production (methionine and serine), and metabolites related to glutathione production (glycine). In addition, acetate, associated with L-cysteine production, demonstrated an increase during the cold-stressed culture. Glutathione plays a crucial role in maintaining redox homeostasis, protecting against reactive oxygen species (ROS), and donating electrons to reductases such as ribonucleotide reductase via NADH (Schmacht et al., 2017). The generation of ROS can stem from the conversion of mitochondrial energy (Tasara and Stephan, 2006), a process modulated by diverse antioxidative enzymes, such as superoxide dismutase, glutathione peroxidase, and glutathione reductase (Blagojevic et al., 2011). Cold-stress can induce ribosomal and mitochondrial damage, disrupting the balance of ROS in energy generation (Tasara and Stephan, 2006). Interestingly, LM demonstrates the capacity to both synthesize glutathione and acquire it from external sources (Sibanda and Buys, 2022), thereby aiding in the alleviation of oxidative stress. Subsequently, synthesis of L-γ-glutamylcysteine using glutamate, L-cysteine, and glycine leads to the production of glutathione (Asantewaa and Harris, 2021). Therefore, glutathione becomes vital for balancing ROS and enhancing stress resistance under cold-stressed conditions, highlighting its significance as a predominant pathway in LM.

While this study cultured LM in Mueller Hinton broth at 8℃ to investigate its metabolic responses under cold stress, this medium does not fully replicate the complexity of actual meat environments or account for the influence of different temperatures on microbial metabolism. According to Kim et al. (2024), although Mueller Hinton broth includes beef extract, the nutrient composition can be compromised during the extraction and processing stages. Furthermore, their study found that LM grown in nutrient-preserving sterilized broth exhibited different intracellular metabolic profiles compared to those grown in Mueller Hinton broth (Kim et al., 2024). Additionally, Cacace et al. (2010) reported that varying temperatures can

lead to different gene expression patterns related to stress responses and metabolic pathways, such as the upregulation of genes associated with glutathione metabolism at higher temperatures. Therefore, further studies are needed to investigate LM in actual meat and under various temperature conditions to better understand its metabolic responses in more realistic environments.

In conclusion, our study focused on the extracellular metabolites of three distinct strains of LM under cold-stressed culture. It was emphasized that the potential of extracellular metabolites examination as a tool for revealing metabolic alterations in LM during the cold-stressed culture. LM showed changes in the expression of energy metabolism-related metabolites (trehalose, lactate, propanoate, acetate, ethanol, and formic acid) and glutathione-related metabolites (acetate, histidine, arginine, proline, glutamate, glycine, serine, and methionine) during cold-stress. The differentiation among each strain (L5, L6, and L9) was confirmed by variations in the levels of lactate, glycerol, acetate, methanol, asparagine, proline, ethanol, and glutamate. Especially, the expression of energy and glutathione metabolisms significantly increased during the lag and log phases of LM growth under cold-stress conditions. This suggests that LM may enhance glutathione metabolism expression as a defensive mechanism in response to cold-stress. The observed changes in the metabolite profiles could be applicable in the food industry, particularly in the rapid detection of foodborne pathogens in cold chain system. In addition, the present results represent the fundamental and essential step toward achieving a holistic comprehension of LM metabolism under cold-stress, utilizing extracellular metabolites. However, to deepen our understanding, future research will need to include a broader range of bacterial strains and environmental conditions.

Acknowledgment

This work was carried out with the support of the National Research Foundation of Korea (NRF) grant funded by the Korea government (MIST) (No. 2022R1A6A3A01085938).

Author contributions

Conceptualization: Kim HJ, Jo C.

Data curation: Kim HJ, Kim HJ.

Formal analysis: Kim HJ.

Methodology: Kim HJ, Kim HJ.

Software: Kim HJ.

Investigation: Kim HJ.

Validation: Kim HJ.

Writing-original draft: Kim HJ, Kim HJ.

Writing - review & editing: Kim HJ, Kim HJ, Jo C.

References

Aertsen A, Michiels CW. 2004. Stress and how bacteria cope with death and survival. Crit Rev Microbiol 30:263-273. https://doi.org/10.1080/10408410490884757

Allen A, Williams MR, Sigman ME. 2019. Application of likelihood ratios and optimal decision thresholds in fire debris analysis based on a partial least squares discriminant analysis (PLS-DA) model. Forensic Chem. 16:100188. https://doi.org/10.1016/j.forc.2019.100188

Asantewaa G, Harris IS. 2021. Glutathione and its precursors in cancer. Curr Opin Biotechnol 68:292-299. https://doi.org/10.1016/j.copbio.2021.03.001

Aung SH, Abeyrathne EDNS, Hossain MA, Jung DY, Kim HC, Jo C, Nam KC. 2023. Comparative Quality Traits, Flavor Compounds, and Metabolite Profile of Korean Native Black Goat Meat. Food Sci Anim Resour 43:639-658. https://doi.org/10.5851/kosfa.2023.e25

Bassey AP, Ye K, Li C, Zhou G. 2021. Transcriptomic-proteomic integration: A powerful synergy to elucidate the mechanisms of meat spoilage in the cold chain. Trends Food Sci Technol 113:12-25. https://doi.org/10.1016/j.tifs.2021.02.051

Blagojevic DP, Grubor-Lajsic GN, Spasic MB. 2011. Cold defence responses: the role of oxidative stress. Front Biosci (Schol Ed) 3:416-427. https://doi.org/10.2741/s161

Cacace G, Mazzeo MF, Sorrentino A, Spada V, Malorni A, Siciliano RA. 2010. Proteomics for the elucidation of cold adaptation mechanisms in Listeria monocytogenes. J Proteomics 73:2021-2030. https://doi.org/10.1016/j.jprot.2010.06.011

Chubukov V, Gerosa L, Kochanowski K, Sauer U. 2014. Coordination of microbial metabolism. Nat Rev Microbiol 12:327-340. https://doi.org/10.1038/nrmicro3238

Cordero N, Maza F, Navea-Perez H, Aravena A, Marquez-Fontt B, Navarrete P, Figueroa G, González M, Latorre M, Reyes-Jara A. 2016. Different transcriptional responses from slow

and fast growth rate strains of *Listeria monocytogenes* adapted to low temperature. Front Microbiol 7:229. https://doi.org/10.3389/fmicb.2016.00229

Dewey-Mattia D. 2018. Surveillance for foodborne disease outbreaks, United States, 2009–2015. MMWR. Surveillance Summaries 67.

Doumith M, Buchrieser C, Glaser P, Jacquet C, Martin P. 2004. Differentiation of the major *Listeria monocytogenes* serovars by multiplex PCR. J Clin Microbiol 42:3819-3822. https://doi.org/10.1128/jcm.42.8.3819-3822.2004

Galindo-Prieto B, Eriksson L, Trygg J. 2014. Variable influence on projection (VIP) for orthogonal projections to latent structures (OPLS). J Chemom 28:623-632. https://doi.org/10.1002/cem.2627

Gonzalez-Garcia RA, McCubbin T, Navone L, Stowers C, Nielsen LK, Marcellin E. 2017. Microbial propionic acid production. Fermentation 3:21. https://doi.org/10.3390/fermentation3020021

Garvie EI. 1980. Bacterial lactate dehydrogenases. Microbiol Rev 44(1):106-139. https://doi.org/10.1128/mr.44.1.106-139.1980

Hain T, Hossain H, Chatterjee SS, Machata S, Volk U, Wagneret S, Brors B, Haas S, Kuenne CT, Billion A, Otten S, Pane-Rarre J, Engelmann S, Chakraborty T. 2008. Temporal transcriptomic analysis of the *Listeria monocytogenes* EGD-e σ B regulon. BMC Microbiol 8:1-12. https://doi.org/10.1186/1471-2180-8-20

Kaur, M, Williams, M, Bissett, A, Ross, T, Bowman, JP. 2021. Effect of abattoir, livestock species and storage temperature on bacterial community dynamics and sensory properties of vacuum packaged red meat. Food Microbiol 94: 103648. https://doi.org/10.1016/j.fm.2020.103648

Kim HC, Ko YJ, Jo C. 2021. Potential of 2D qNMR spectroscopy for distinguishing chicken breeds based on the metabolic differences. Food Chem 342:1-9. https://doi.org/10.1016/j.foodchem.2020.128316

Kim HC, Baek KH, LeeYE, Kang T, Kim HJ, Lee D, Jo C. 2022. Using 2D qNMR analysis to distinguish between frozen and frozen/thawed chicken meat and evaluate freshness. npj Sci Food 6:44. https://doi.org/10.1038/s41538-022-00159-x

Kim HJ, Kim HJ, Hong H, Jo C. 2022. Metabolomic approaches for the detection of *Listeria monocytogenes* and *Staphylococcus aureus* in culture media. LWT 171:114117. https://doi.org/10.1016/j.lwt.2022.114117

Kim HJ, Kim HJ, Hong H, Jo C. 2024. Meat-derived broth as a novel culture medium for metabolomic study of bacteria in meat. LWT 116254. https://doi.org/10.1016/j.lwt.2024.116254

Kramarenko T, Roasto M, Meremäe K, Kuningas M, Põltsama P, Elias T. 2013 *Listeria monocytogenes* prevalence and serotype diversity in various foods. Food Control 30:24-29. https://doi.org/10.1016/j.foodcont.2012.06.047

Mataragas, M., Drosinos, E. H., Vaidanis, A., & Metaxopoulos, I. 2006. Development of a predictive model for spoilage of cooked cured meat products and its validation under constant and dynamic temperature storage conditions. J Food Sci 71:157-167. https://doi.org/10.1111/j.1750-3841.2006.00058.x

Nightingale KK, Windham K, Wiedmann M. 2005. Evolution and molecular phylogeny of *Listeria monocytogenes* isolated from human and animal listeriosis cases and foods. J Bacteriol 187:5537-5551. https://doi.org/ 10.1128/jb.187.16.5537-5551.2005

Painter JA, Hoekstra RM, Ayers T, Tauxe RV, Braden CR, Angulo FJ, Griffin PM. 2013. Attribution of foodborne illnesses, hospitalizations, and deaths to food commodities by

476 using outbreak data, United States, 1998–2008. Emerg Infect Dis 19:407.
477 https://doi.org/10.3201/eid1903.111866
478 Park, S. Y., Kim, Y. J., Lee, H. C., Yoo, S. S., Shim, J. H., & Chin, K. B. 2008. Effects of
479 pork meat cut and packaging type on lipid oxidation and oxidative products during
480 refrigerated storage (8 C). J Food Sci 73:127-134. https://doi.org/10.1111/j.1750-
481 3841.2007.00656.x
482 Pinu FR, Villas-Boas SG, Aggio R. 2017. Analysis of intracellular metabolites from
483 microorganisms: quenching and extraction protocols. Metabolites 7:53.
484 https://doi.org/10.3390/metabo7040053
485 Pinu FR, Villas-Boas SG. 2017. Extracellular microbial metabolomics: the state of the art.
486 Metabolites 7:43. https://doi.org/10.3390/metabo7030043
487 Rinehart E, Newton E, Marasco MA, Beemiller K, Zani A, Muratore MK, Weis J,
488 Steinbicker N, Wallace N, Sun Y. 2018. *Listeria monocytogenes* response to propionate is
489 differentially modulated by anaerobicity. Pathogens 7:60.
490 https://doi.org/10.3390/pathogens7030060
491 Robador A, LaRowe DE, Finkel SE, Amend JP, Nealson KH. 2018. Changes in microbial
492 energy metabolism measured by nanocalorimetry during growth phase transitions. Front
493 Microbiol 9:109. https://doi.org/10.3389/fmicb.2018.00109
494 Roccato, A., Uyttendaele, M., Cibin, V., Barrucci, F., Cappa, V., Zavagnin, P., Longo, A.,
495 Catellani, P, & Ricci, A. 2015. Effects of domestic storage and thawing practices on
496 Salmonella in poultry-based meat preparations. J Food Prot 78:2117-2125.
497 https://doi.org/10.4315/0362-028X.JFP-15-048
498 Rosenow EM, Marth EH. 1987. Growth of *Listeria monocytogenes* in skim, whole and
499 chocolate milk, and in whipping cream during incubation at 4, 8, 13, 21 and 35° C. J Food
500 Prot 50:452-460. https://doi.org/10.4315/0362-028X-50.6.452

501 Sauer JD, Herskovits AA, O'Riordan MX. 2019. Metabolism of the gram-positive bacterial
502 pathogen *Listeria monocytogenes*: Gram-Positive Pathogens. Washington (DC): ASM
503 press. https://doi.org/10.1128/9781683670131.ch54
504 Schär J, Stoll R, Schauer K, Loeffler DI, Eylert E, Joseph B, Eisenreich W, Fuchs TM,
505 Goebel W. 2010. Pyruvate carboxylase plays a crucial role in carbon metabolism of extra-
506 and intracellularly replicating *Listeria monocytogenes*. J. Bacteriol 192:1774-1784.
507 https://doi.org/10.1128/jb.01132-09
508 Schmacht M, Lorenz E, Senz M. 2017. Microbial production of glutathione. World J
509 Microbiol Biotechnol 33:1-13. https://doi.org/10.1007/s11274-017-2277-7
510 Sibanda T, Buys E M. 2022. *Listeria monocytogenes* pathogenesis: The role of stress
511 adaptation. Microorganisms 10:1522. https://doi.org/10.3390/microorganisms10081522
512 Sørheim, O., Nissen, H., & Nesbakken, T. 1999. The storage life of beef and pork packaged
513 in an atmosphere with low carbon monoxide and high carbon dioxide. Meat Sci 52:157-
514 164. https://doi.org/10.1016/S0309-1740(98)00163-6
515 Tasara T, Stephan R. 2006. Cold stress tolerance of *Listeria monocytogenes*: a review of
516 molecular adaptive mechanisms and food safety implications. J Food Prot 69:1473-1484.
517 https://doi.org/10.4315/0362-028X-69.6.1473
518 Yoon SH, Kim GB. 2022. Inhibition of *Listeria monocytogenes* in Fresh Cheese Using a
519 Bacteriocin-Producing *Lactococcus lactis* CAU2013 Strain. Food Sci Anim Resour
520 42:1009. https://doi.org/10.5851/kosfa.2022.e48
521 Yu M, Jiang C, Meng Y, Wang F, Qian J, Fei F, Yin Z, Zhao W, Zhao Y, Liu H. 2023. Effect
522 of low temperature on the resistance of *Listeria monocytogenes* and *Escherichia coli* O157:
523 H7 to acid electrolyzed water. Food Res Int 168:112776.
524 https://doi.org/10.1016/j.foodres.2023.112776

525 Vanaporn M, Titball RW. 2020. Trehalose and bacterial virulence. Virulence 11:1192-1202.
526 https://doi.org/10.1080/21505594.2020.1809326
527 Willey JM, Sherwood L, Woolverton C. 2013. Prescott's microbiology. 9th ed. New York
528 (NY): McGraw Hill Higher Education.
529 Xia J, Wishart DS. 2011. Web-based inference of biological patterns, functions and pathways
530 from metabolomic data using MetaboAnalyst. Nat Protoc 6:743-760.
531 https://doi.org/10.1038/nprot.2011.319
532

Figure legends

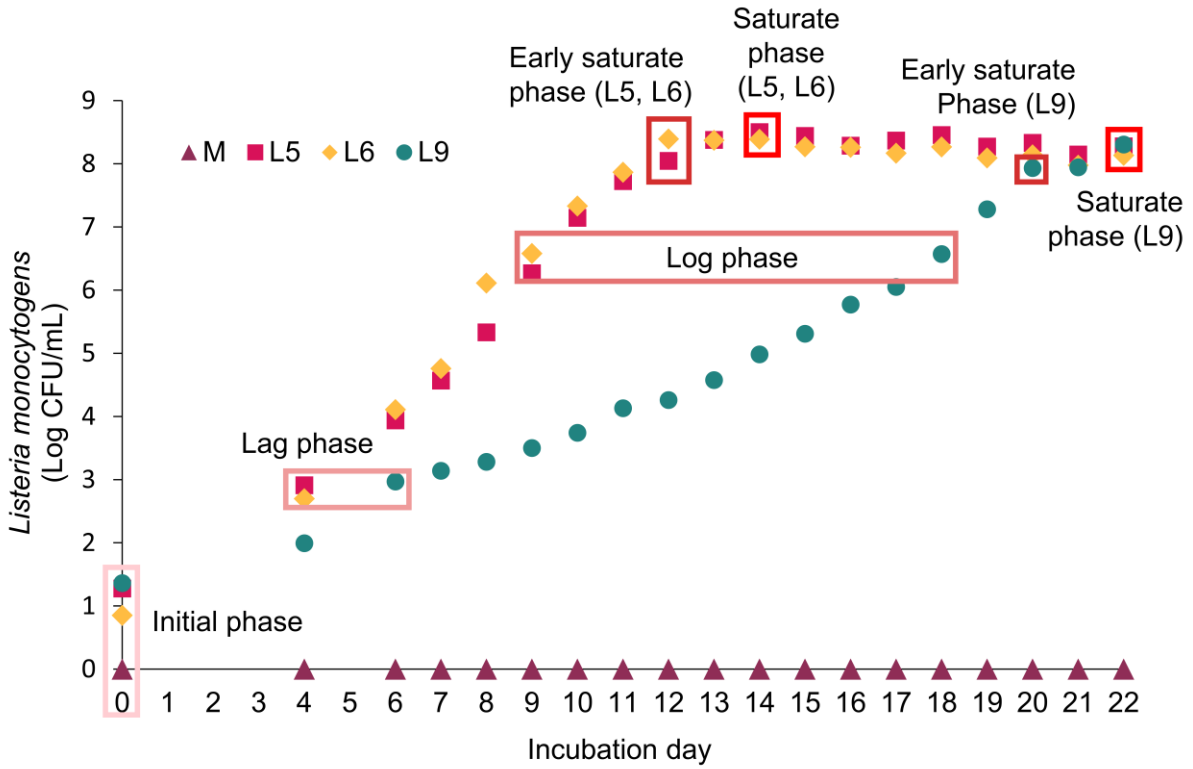

Fig. 1. Growth curve of different strains of *Listeria monocytogenes* (LM) at 8℃. M, un inoculated Mueller Hinton broth; L5, *L. monocytogenes* NCCP 15743; L6, *L. monocytogenes* NCCP 16594; L9, *L. monocytogenes* ATCC 19111. Initial phase, microorganisms was inoculated at 1 log CFU /mL. Lag phase, the culture medium immediately before reaching 3 log CFU/mL. Log phase, culture medium above 6 log CFU/mL. Early saturate phase, culture medium above 8 log CFU/mL. Saturate phase, 2 days after reaching 8 log CFU/mL.

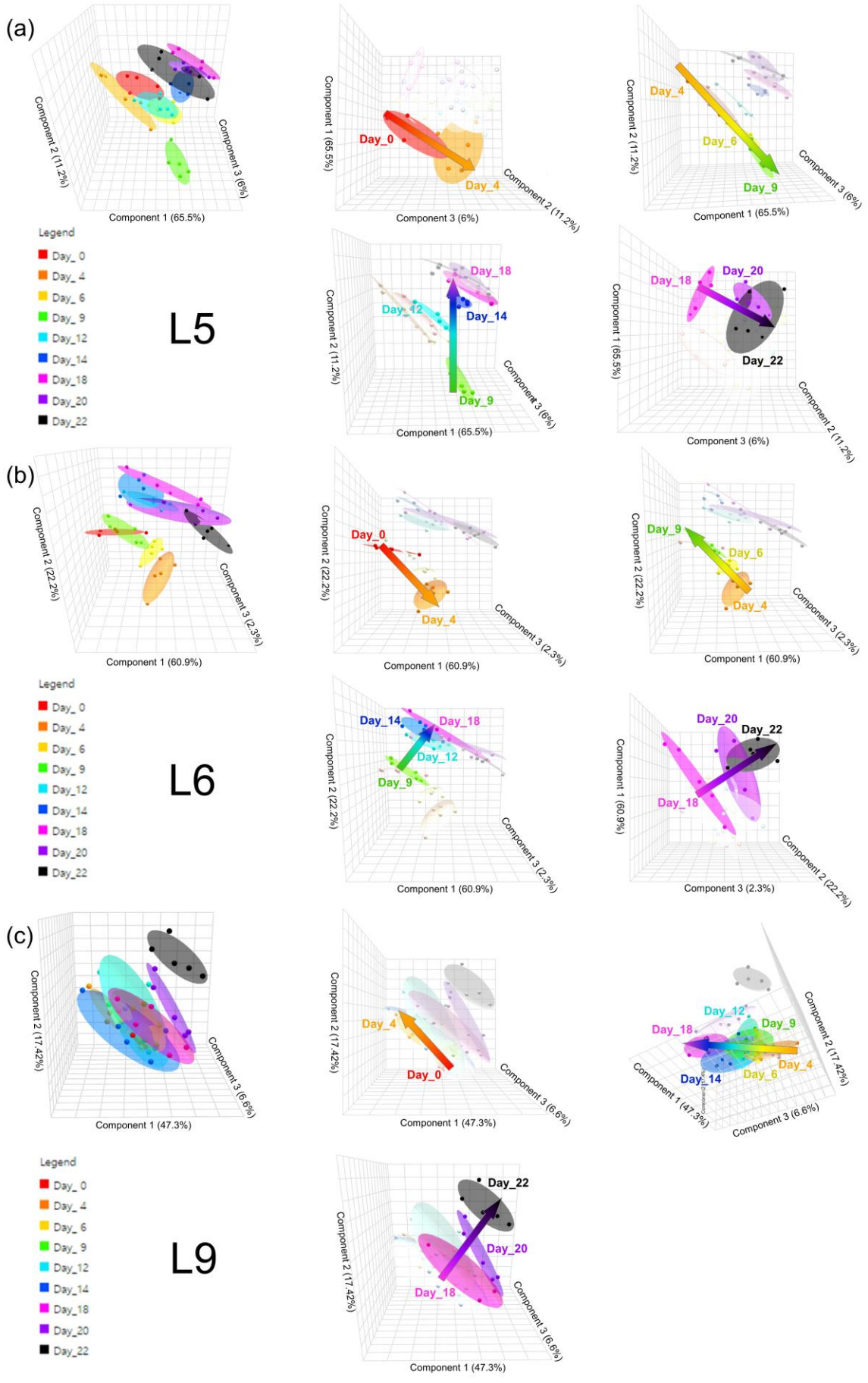
(a)
Component 1 (65.5%)
Component 2 (11.2%)
Component 3 (6%)
Day_0
Day_4
Day_6
Day_9
Legend
Day_ 0
Day_ 4
Day_ 6
Day_ 9
Day_12
Day_14
Day_18
Day_20
Day_22
L5
Day_12
Day_18
Day_14
Day_20
Day_22
(b)
Component 1 (60.9%)
Component 2 (22.2%)
Component 3 (2.3%)
L6
(c)
Component 1 (47.3%)
Component 2 (17.42%)
Component 3 (6.6%)
L9

543 Fig. 2. Pattern changes of *L. monocytogenes* extracellular metabolites analyzed by PLS-DA.

544 Color arrows indicate the segregation tendency. L5, *L. monocytogenes* NCCP 15743(a); L6, *L.*

545 *monocytogenes* NCCP 16594 (b); L9, *L. monocytogenes* ATCC 19111 (c).

546

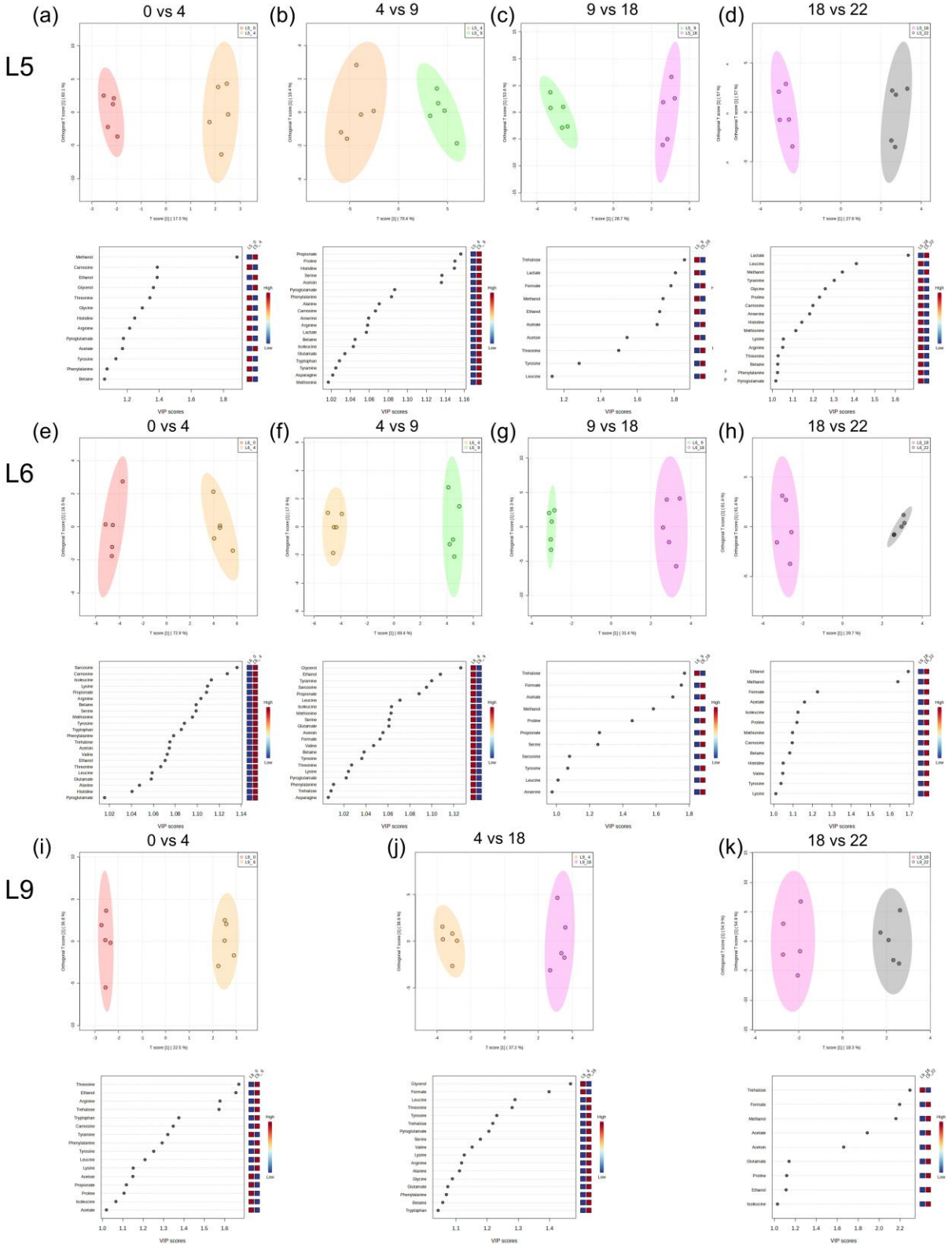

Fig. 3. OPLS-DA results for pattern changes of *L. monocytogenes* extracellular metabolites. L5, *L. monocytogenes* NCCP 15743(a-d); L6, *L. monocytogenes* NCCP 16594 (e-h); L9, *L. monocytogenes* ATCC 19111 (i-k).

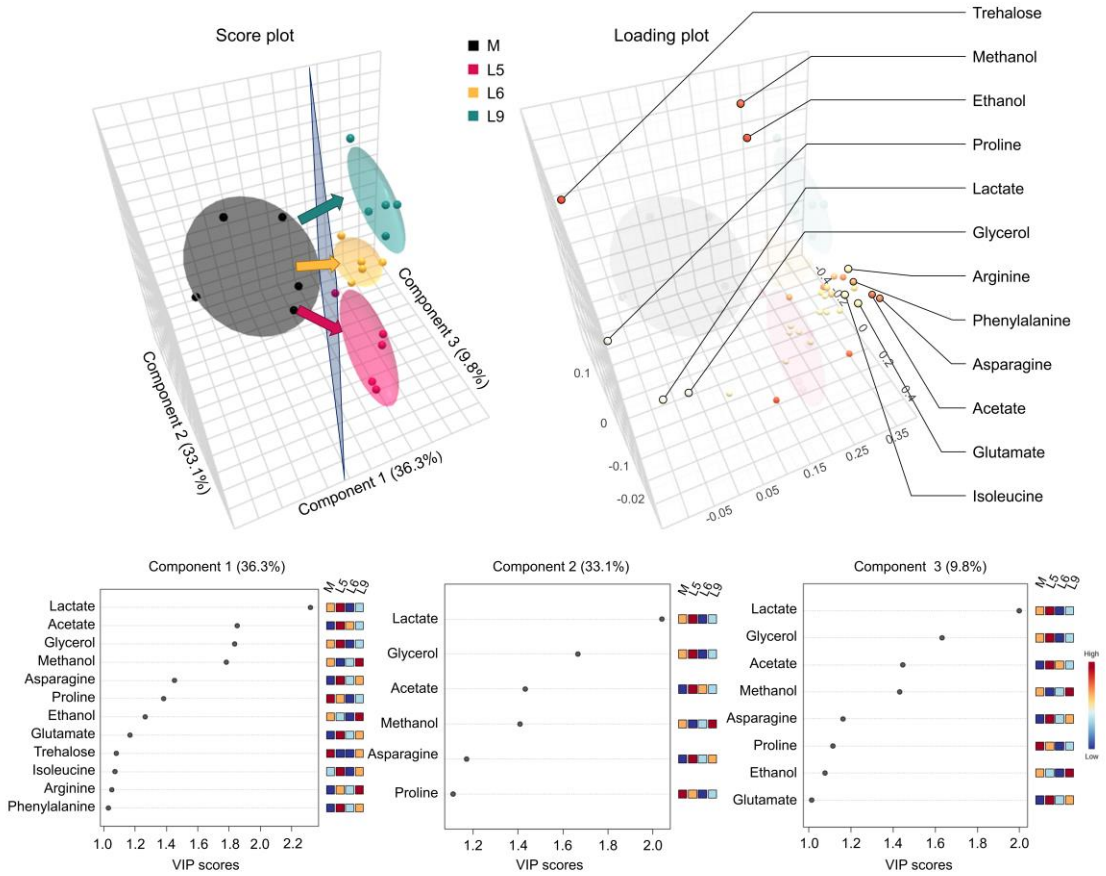

Fig. 4. PLS-DA analysis of extracellular metabolites in different strains of *L. monocytogenes* under cold-stress. Analysis conducted at saturated phase. M, un inoculated Mueller Hinton broth; L5, *L. monocytogenes* NCCP 15743; L6, *L. monocytogenes* NCCP 16594; L9, *L. monocytogenes* ATCC 19111.

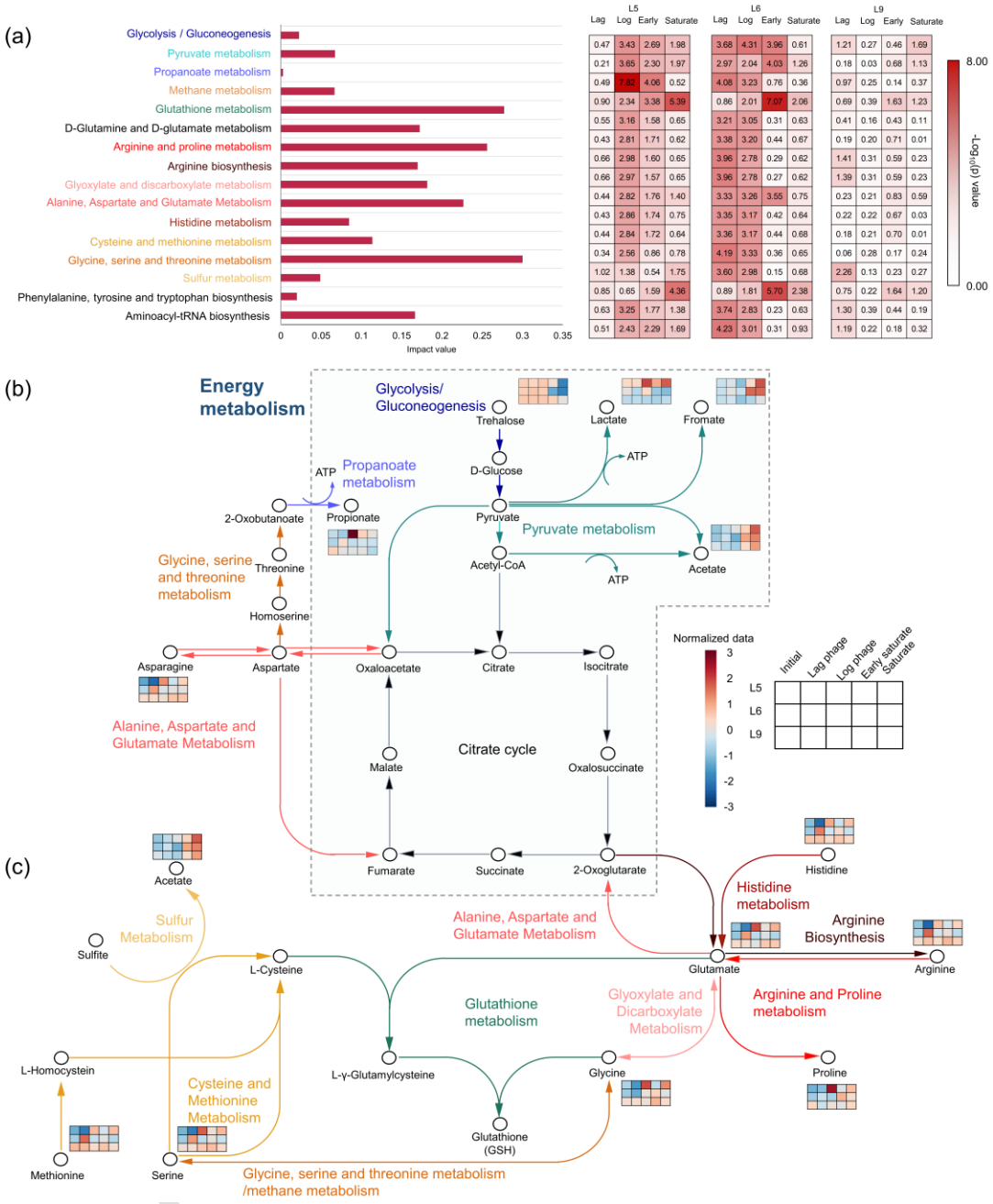

Fig. 5. Metabolic pathway analysis of *L. monocytogenes.* (a) Metabolic expression level of *L. monocytogenes* according to growth phases, with the pathway expression values compared to the uninoculated culture medium (P<0.05). (b) Energy metabolism. (c) Glutathione-related metabolism. Represented by colored squares indicating the concentration of the normalized metabolites at different phases (initial, lag, log, early saturate, and saturate) for *L. monocytogenes* strains. L5, *L. monocytogenes* NCCP 15743; L6, *L. monocytogenes* NCCP 16594; L9, *L. monocytogenes* ATCC 19111.

565 Table S1. Isolated strains information of *Listeria monocytogenes* from National Culture
566 Collection for Pathogens

Name	Source	Genotype	Serotype	Antibiotic Susceptibility[b]
ATCC 19111	Poultry	Li 20	1/2a	
NCCP 15743	Blood	MLST[a] ST New (7-15-15-10-6-14-9)	1/2a, Antigen O:1,2 H:a,b	Ampicillin: S (0.25 μg/mL) Penicillin G: S (0.5 μg/mL) Erythromycin: S (0.5 μg/mL) Vancomycin: S (2 μg/mL) Tetracycline: R (16 μg/mL) Trimethoprim-Sulfamethoxazole: S (0.5/9.5 μg/mL) Rifampin: S (0.5 μg/mL) Linezolid: S (4 μg/mL)
NCCP 16594	Blood	MLST ST 2687	1/2a, Antigen O:1,2 H:a,b	Ampicillin: S (0.25 μg/mL) Penicillin G: S (0.25 μg/mL) Erythromycin: S (0.5 μg/mL) Vancomycin: S (2 μg/mL) Tetracycline: R (4 μg/mL) Trimethoprim-Sulfamethoxazole: S (0.5/9.5 μg/mL) Rifampin: S (0.5 μg/mL) Linezolid: S (4 μg/mL)

567 [a]MLST, Multilocus Sequence Typing.

568 [b]Antibiotic susceptibility is denoted as "S" (Susceptible) or "R" (Resistant), with the Minimum
569 Inhibitory Concentrations (MICs) provided in μg/mL.

570 Table S2. ^{1}H and ^{13}C nuclear magnetic resonance (NMR) peak assignments for identified
571 metabolites using Chenomx, correlated spectroscopy (COZY), and heteronuclear single
572 quantum coherence (HSQC) spectroscopy

No.	Metabolites	Chemical shift ($\delta^{1}H$, $\delta^{13}C$; ppm)
1	Acetate	(1.93, 26.18)
2	Acetoin	(1.36, 20.92), (2.21, 27.55), (4.42, 75.69)
3	Alanine	(1.50, 18.97), (3.81, 53.23)
4	Anserine	(2.71, 34.85), (3.07, 28.65), (3.23, 28.65), (3.23, 38.32), (3.26, 28.83), (3.82, 35.49), (4.51, 56.22), (7.18. 122.10), (8.40, 138.62)
5	Arginine	(1.68, 26.45), (1.91, 30.49), (3.24, 43.32), (3.76, 57.26)
6	Asparagine	(2.92, 37.43), (2.95, 37.34), (2.98, 37.42), (4.03, 54.11)
7	Betaine	(3.28, 56.22), (3.93, 69.04)
8	Carnosine	(2.73, 34.80), (3.08, 30.40), (3.22, 30.27), (3.23, 39.18), (4.49, 57.27), (7.18, 119.64)
9	Ethanol	(1.15, 19.50), (3.67, 60.27)
10	Formate	(8.39, 172.41*)
11	Glutamate	(2.09, 29.78), (2.14, 29.72), (2.37, 36.21), (3.75, 57.27)
12	Glycerol	(3.56, 65.41), (3.65, 65.49), (3.77, 74.98)
13	Glycine	(3.59, 44.27)
14	Histidine	(3.21, 30.08), (3.27, 30.20), (3.29, 30.20), (4.00, 57.28), (7.14, 119.99), (8.03, 138.37)
15	Isoleucine	(0.95, 13.88), (0.96, 26.88) (1.02, 17.57), (1.28, 27.25), (1.99, 38.65), (3.69, 62.37)
16	Lactate	(1.35, 71.33), (4.10, 71.15)
17	Leucine	(0.96, 23.74), (0.97, 24.94), (1.70, 42.59), (1.72, 27.06), (1.75, 42.61), (3.75, 56.22)
18	Lysine	(1.49, 24.04), (1.72, 29.15), (1.88, 32.65), (3.02, 42.12), (3.75, 57.45)
19	Methnanol	(3.37, 51.43)
20	Methionine	(2.14, 16.69), (2.15, 32.43), (2.21, 32.41), (2.65, 31.60), (3.88, 56.57)
21	Phenylalanine	(4.01, 58.86), (7.31, 132.29), (7.35, 130.54), (7.41, 131.94)
22	Proline	(2.03, 26.56), (2.09, 31.64), (2.36, 31.81), (3.36, 48.85), (3.43, 48.85), (4.15, 63.95)
23	Propionate	(1.04, 12.99), (2.17, 33.48)
24	Pyroglutamate	(2.01, 27.98), (2.38, 32.28), (2.49, 27.98), (4.16, 60.97)
25	Sarcosine	(2.72, 35.57), (3.59, 53.50)
26	Serine	(3.87, 59.21), (3.97, 63.06), (4.01, 63.06)
27	Threonine	(1.35, 21.79), (4.28, 68.69)
28	Trehalose	(3.44, 72.47), (3.64, 73.78), (3.76, 63.31), (3.81, 74.88), (3.85, 75.35), (3.86, 63.34), (5.18, 95.98)
29	Tryptophan	(4.03, 30.05), (7.43, 114.72), (7.65, 121.23)
30	Tyramine	(2.93, 34.63), (3.26, 43.70), (6.90, 118.55), (7.22, 133.06)
31	Tyrosine	(3.07, 38.43), (3.96, 58.86), (3.95, 58.86), (6.89, 118.77), (7.20, 133.70)
32	Valine	(1.00, 19.50), (1.05, 20.73), (2.29, 31.98), (3.62, 63.25)

573 *Identified through Chenomx and the human metabolites database (HMDB).
574

575 Table S3. Metabolites changes in *L. monocytogenes* NCCP 15743 by Growth phase

Compound	M	Initial	Lag	Log	Early	Saturate	SEM
Acetate	0.564^{cd}	0.489^{c}	0.563^{cd}	0.625^{bcd}	0.737^{b}	1.064^{a}	0.0288
Acetoin	0.293^{b}	0.279^{b}	0.264^{b}	0.541^{a}	0.32^{b}	0.346^{b}	0.0235
Alanine	0.915^{cb}	0.802^{cd}	0.731^{d}	1.135^{a}	0.967^{abc}	1.107^{ab}	0.0430
Anserine	0.565^{a}	0.459^{b}	0.445^{b}	0.636^{a}	0.598^{a}	0.649^{a}	0.0239
Arginine	3.348^{ab}	3.199^{ab}	2.651^{b}	3.976^{a}	3.552^{a}	3.867^{a}	0.1965
Asparagine	0.833^{b}	0.769^{b}	0.69^{b}	1.121^{a}	0.896^{ab}	1.073^{a}	0.0521
Betaine	0.142^{abc}	0.134^{bc}	0.114^{c}	0.175^{a}	0.138^{bc}	0.155^{ab}	0.0082
Carnosine	0.502^{ab}	0.475^{ab}	0.37^{b}	0.614^{a}	0.484^{ab}	0.6^{a}	0.0327
Ethanol	0.956^{ab}	0.731^{c}	0.847^{bc}	1.051^{a}	0.812^{bc}	0.859^{bc}	0.0409
Formate	0.158^{bc}	0.127^{bc}	0.143^{bc}	0.083^{c}	0.198^{b}	0.583^{a}	0.0182
Glutamate	2.754^{bc}	2.738^{bc}	2.398^{c}	4.117^{a}	3.162^{abc}	3.529^{ab}	0.2304
Glycerol	1.283^{b}	0.906^{b}	1.238^{b}	1.353^{b}	1.128^{b}	3.216^{a}	0.3099
Glycine	0.294^{abc}	0.263^{bc}	0.235^{c}	0.371^{a}	0.27^{bc}	0.34^{ab}	0.0181
Histidine	0.588^{abc}	0.554^{bc}	0.463^{c}	0.719^{a}	0.602^{abc}	0.692^{ab}	0.0328
Isoleucine	2.032^{bc}	1.96^{bc}	1.734^{c}	3.007^{a}	2.248^{bc}	2.463^{ab}	0.1688
Lactate	1.194^{c}	1.04^{c}	1.03^{c}	1.725^{a}	1.265^{bc}	1.616^{ab}	0.0885
Leucine	6.783^{ab}	5.99^{b}	5.479^{b}	8.265^{a}	6.932^{ab}	8.077^{a}	0.3724
Lysine	20.946^{ab}	19.47^{ab}	17.524^{b}	24.559^{b}	20.543^{ab}	24.149^{a}	1.1230
Methanol	0.027^{bc}	0.022^{c}	0.032^{bc}	0.043^{a}	0.034^{ab}	0.023^{bc}	0.0024
Methionine	1.389^{ab}	1.25^{bc}	1.153^{b}	1.591^{a}	1.426^{ab}	1.585^{abc}	0.0747

Phenylalanine	3.449^{ab}	3.093^{bc}	2.784^{c}	4.157^{a}	3.573^{ab}	4.074^{a}	0.1503
Proline	0.183^{abc}	0.088^{bc}	0.085^{b}	0.276^{a}	0.126^{bc}	0.154^{bc}	0.0197
Propionate	0.108^{bc}	0.107^{bc}	0.095^{c}	0.462^{a}	0.174^{b}	0.132^{bc}	0.0188
Pyroglutamate	3.171^{cd}	2.762^{cd}	2.412^{d}	4.176^{a}	3.399^{abc}	3.705^{ab}	0.1804
Sarcosine	0.129^{abc}	0.12^{bc}	0.112^{c}	0.17^{a}	0.14^{abc}	0.16^{ab}	0.0103
Serine	1.900^{bc}	1.547^{cd}	1.327^{d}	2.604^{a}	1.956^{bc}	2.194^{ab}	0.1206
Threonine	7.493^{ab}	7.209^{ab}	5.936^{b}	7.115^{b}	7.596^{ab}	8.953^{a}	0.3907
Trehalose	0.981^{ab}	0.93^{ab}	0.832^{b}	1.157^{a}	0.528^{c}	0^{d}	0.0662
Tryptophan	1.104^{ab}	1.038^{b}	0.929^{b}	1.366^{a}	1.202^{ab}	1.334^{a}	0.0651
Tyramine	0.161^{bc}	0.138^{c}	0.126^{c}	0.196^{ab}	0.166^{abc}	0.212^{a}	0.0113
Tyrosine	0.689^{ab}	0.684^{ab}	0.573^{b}	0.741^{a}	0.719^{ab}	0.814^{a}	0.0374
Valine	1.916^{bc}	1.728^{c}	1.606^{c}	2.405^{a}	1.902^{bc}	2.307^{ab}	0.1134

576 SEM, standard error of the mean.

577 $^{a\text{-}d}$ Means with different letters within the same row are significantly different ($P < 0.05$).

578 Table S4. Metabolites changes in *L. monocytogenes* NCCP 16594 by Growth phase

Compound	M	Initial	Lag	Log	Early	Saturate	SEM
Acetate	0.564^{b}	0.496^{b}	0.579^{b}	0.449^{b}	0.857^{a}	0.952^{a}	0.0274
Acetoin	0.293^{b}	0.274^{b}	0.390^{a}	0.284^{b}	0.303^{b}	0.294^{b}	0.0132
Alanine	0.915^{b}	0.882^{b}	1.154^{a}	0.947^{b}	0.951^{b}	0.906^{b}	0.0321
Anserine	0.565^{b}	0.573^{ab}	0.673^{a}	0.545^{b}	0.574^{ab}	0.566^{b}	0.0253
Arginine	3.348^{b}	3.289^{b}	4.562^{a}	3.555^{b}	3.679^{b}	3.391^{b}	0.1604
Asparagine	0.833^{b}	0.864^{b}	1.093^{a}	0.915^{b}	0.935^{ab}	0.939^{ab}	0.0349
Betaine	0.142^{b}	0.140^{b}	0.186^{a}	0.145^{b}	0.140^{b}	0.129^{b}	0.0051
Carnosine	0.502^{b}	0.463^{b}	0.696^{a}	0.527^{b}	0.565^{b}	0.485^{b}	0.0235
Ethanol	0.956^{b}	0.847^{b}	1.382^{a}	0.791^{b}	0.790^{b}	0.836^{b}	0.0541
Formate	0.158^{a}	0.123^{a}	0.153^{a}	0.120^{a}	0.502^{b}	0.503^{b}	0.0162
Glutamate	2.754^{b}	2.708^{b}	3.662^{a}	2.871^{b}	3.037^{b}	2.828^{b}	0.1138
Glycerol	1.283^{b}	1.616^{b}	6.377^{a}	0.657^{b}	1.644^{b}	0.690^{b}	0.5995
Glycine	0.294	0.259	0.248	0.290	0.305	0.284	0.0154
Histidine	0.588^{b}	0.564^{b}	0.764^{a}	0.607^{b}	0.649^{ab}	0.597^{b}	0.0277
Isoleucine	2.032^{b}	1.934^{b}	2.681^{a}	2.076^{b}	2.123^{b}	2.008^{b}	0.0718
Lactate	1.194^{a}	0.923^{bc}	0.762^{abc}	1.038^{ab}	0.692^{d}	0.650^{d}	0.0489
Leucine	6.783^{b}	6.620^{b}	8.732^{a}	6.984^{b}	7.255^{b}	6.840^{b}	0.2288
Lysine	20.946^{b}	20.382^{b}	27.584^{a}	21.462^{b}	22.473^{b}	20.242^{b}	0.8220
Methanol	0.027^{b}	0.029^{ab}	0.035^{a}	0.028^{b}	0.027^{b}	0.023^{b}	0.0013
Methionine	1.389^{b}	1.326^{b}	1.775^{a}	1.388^{b}	1.450^{b}	1.356^{b}	0.0487

Phenylalanine	3.449[b]	3.425[b]	4.540[a]	3.590[b]	3.713[b]	3.472[b]	0.1389
Proline	0.183[a]	0.092[c]	0.109[bc]	0.093[c]	0.160[ab]	0.128[bc]	0.0101
Propionate	0.108[b]	0.099[b]	0.144[a]	0.108[b]	0.117[b]	0.112[b]	0.0041
Pyroglutamate	3.171[b]	3.065[b]	3.973[a]	3.235[b]	3.291[b]	3.090[b]	0.1200
Sarcosine	0.129[b]	0.118[b]	0.172[a]	0.124[b]	0.137[b]	0.125[b]	0.0050
Serine	1.900[b]	1.631[b]	2.341[a]	1.736[b]	1.928[b]	1.772[b]	0.0796
Threonine	7.493[b]	7.500[b]	9.940[a]	7.824[b]	8.007[b]	7.420[b]	0.3064
Trehalose	0.981[b]	0.957[b]	1.282[a]	1.004[b]	0.025[c]	0.000[c]	0.0319
Tryptophan	1.104[b]	1.129[b]	1.532[a]	1.201[b]	1.229[b]	1.120[b]	0.0521
Tyramine	0.161[b]	0.168[b]	0.210[a]	0.171[b]	0.179[ab]	0.180[ab]	0.0060
Tyrosine	0.689[b]	0.684[b]	0.925[a]	0.694[b]	0.735[b]	0.706[b]	0.0299
Valine	1.916[b]	1.834[b]	2.435[a]	1.909[b]	2.019[b]	1.872[b]	0.0714

579 SEM, standard error of the mean.

580 [a-c] Means with different letters within the same row are significantly different ($P < 0.05$).

581 Table S5. Metabolites changes in *L. monocytogenes* ATCC 19111 by Growth phase

Compound	M	Initial	Lag	Log	Early	Saturate	SEM
Acetate	0.564^{b}	0.604^{b}	0.549^{b}	0.519^{b}	0.698^{ab}	0.903^{a}	0.0494
Acetoin	0.293^{ab}	0.360^{b}	0.332^{b}	0.260^{a}	0.317^{ab}	0.299^{ab}	0.0155
Alanine	0.915	1.030	1.066	1.012	1.032	0.988	0.0425
Anserine	0.565	0.598	0.603	0.594	0.631	0.621	0.0251
Arginine	3.348^{b}	3.732^{ab}	3.967^{ab}	3.780^{ab}	4.053^{a}	3.889^{ab}	0.1390
Asparagine	0.833^{b}	0.966^{ab}	0.979^{ab}	0.958^{ab}	1.025^{a}	1.026^{a}	0.0315
Betaine	0.142	0.163	0.166	0.161	0.158	0.146	0.0069
Carnosine	0.502	0.573	0.606	0.533	0.562	0.510	0.0217
Ethanol	0.956	0.945	1.106	0.987	0.936	1.145	0.0633
Formate	0.158^{a}	0.118^{abc}	0.129^{ab}	0.082^{c}	0.102^{bc}	0.150^{a}	0.0069
Glutamate	2.754^{b}	3.230^{ab}	3.180^{ab}	3.084^{ab}	3.383^{a}	3.380^{a}	0.1127
Glycerol	1.283^{bc}	2.335^{ab}	2.459^{a}	0.975^{c}	0.760^{c}	0.804^{c}	0.2602
Glycine	0.294	0.295	0.298	0.294	0.320	0.302	0.0153
Histidine	0.588	0.681	0.689	0.653	0.686	0.667	0.0293
Isoleucine	2.032	2.415	2.268	2.222	2.403	2.421	0.0886
Lactate	1.194^{a}	0.788^{b}	0.785^{b}	0.785^{b}	0.735^{b}	0.797^{b}	0.0740
Leucine	6.783	7.087	7.382	7.657	7.614	7.246	0.3300
Lysine	20.946	23.730	24.568	23.822	24.531	23.147	1.0041
Methanol	0.027^{bc}	0.027^{bc}	0.029^{bc}	0.021^{c}	0.032^{ab}	0.041^{a}	0.0021
Methionine	1.389	1.597	1.593	1.523	1.583	1.507	0.0744

Phenylalanine	3.449[b]	3.907[ab]	4.053[ab]	3.859[ab]	4.116[a]	4.013[ab]	0.1288
Proline	0.183[b]	0.139[ab]	0.105[a]	0.125[ab]	0.116[ab]	0.136[ab]	0.0100
Propionate	0.108[b]	0.162[a]	0.130[ab]	0.125[ab]	0.129[ab]	0.111[ab]	0.0130
Pyroglutamate	3.171	3.480	3.602	3.519	3.651	3.526	0.1496
Sarcosine	0.129	0.144	0.147	0.137	0.147	0.138	0.0068
Serine	1.900	1.933	1.963	1.980	2.161	2.000	0.0774
Threonine	7.493	8.217	8.691	8.557	8.884	8.412	0.3732
Trehalose	0.981[ab]	1.066[a]	1.126[a]	1.107[a]	0.871[b]	0.323[c]	0.0328
Tryptophan	1.104	1.290	1.346	1.320	1.348	1.294	0.0601
Tyramine	0.161[b]	0.201[a]	0.191[ab]	0.176[ab]	0.201[a]	0.186[ab]	0.0063
Tyrosine	0.689[b]	0.760[ab]	0.798[ab]	0.807[ab]	0.832[a]	0.792[ab]	0.0261
Valine	1.916	2.093	2.110	2.055	2.225	2.163	0.0703

582 SEM, standard error of the mean.

583 [a-c] Means with different letters within the same row are significantly different ($P < 0.05$).

584

585